Experimental observations of large changes in electron density distributions in β-Ge

Rui Li,[1,2,*] Jing Liu,[1] Dmitry Popov,[3] Changyong Park [3] Yue Meng,[3] and Guoyin Shen [3,†]

[1]*Institute of High Energy Physics, Chinese Academy of Sciences, Beijing 100049, China*
[2]*Geophysical Laboratory, Carnegie Institution for Science, Washington DC 20015, USA*
[3]*HPCAT, X-ray Science Division, Argonne National Laboratory, Argonne, Illinois 60439, USA*

The electron density distributions in β-Ge have been experimentally determined at *in situ* high-pressure conditions using synchrotron diffraction techniques in a diamond anvil cell. Upon decompression, the electron density along the *c* axis in tetragonal β-Ge displays a sudden drop at 10–11 GPa close to that of the structural α-β transition, while the β-Ge samples remain as single crystals until transforming to metastable Ge phases around 6.7–8.5 GPa. In contrast to the covalently bonded α-Ge that displays only a weak participation of *d* electrons in the valence band under compression above 7.7 GPa, our experimental results suggest that a large change in *d*-orbital participation can occur in the β-Ge lattice which has mixed covalent and metallic bonding. The β-Ge below 10 GPa may display large fluctuations in electronic properties, which sheds light for exploring novel materials with intriguing electronic and optical properties.

I. INTRODUCTION

Under pressure, Ge undergoes a semiconducting-metallic transition around 11 GPa from diamond structure (α-Ge) to β-tin structure (β-Ge). Similar transitions are also observed in Group IV elements (Si, α-Sn), III-V compounds (GaP, AlSb, GaSb, InSb, GaAs), and II-VI compounds (ZnS, ZnSe, CdTe) at high pressures [1–6]. The α-β transition in Ge is accompanied by a large change (∼19%) in molar volume and a sudden increase in metallic character in the bonding [7,8]. One important feature of the α-β transition is the participation of 4*d* electrons in bonding in β-Ge, by breaking the sp^3 directional bonding in α-Ge [9–15]. In the metallic β-Ge, the Ge atom is approximately sixfold coordinated, with four covalently bonded along the *ab* plane and two metallically bonded along the *c* direction. Under decompression, the α-β transition is irreversible, with metastable phases observed upon pressure release [16,17], except one report [18] where the back transformation to α-Ge is observed. Several metastable phases (such as rhombohedral r8-Ge, body-centered cubic bc8-Ge, hexagonal diamond hd-Ge, and simple tetragonal st12-Ge) are reported to occur upon decompression [19–23], with attractive electronic and optical properties [14,22]. The formation of the metastable phases is related to the experimental pathways and the hydrostaticity of the sample environment. For example, quasihydrostatic conditions result in the nucleation of r8-Ge, followed by bc8-Ge and hd-Ge, while the presence of shear yields st12-Ge [17].

Recently, the electron density distributions (EDDs) in α-Ge under compression show that the sp^3 bonding is enhanced with increasing pressure up to 7.7 GPa, above which an increased participation of *d* electrons in the valence band occurs [24]. This result suggests that the electronic changes happen at pressures far below the structural α-β transition pressure (∼11 GPa), with the weakening of the covalent bonds preceding the structural phase transition. On the other hand upon decompression, β-Ge can exist at pressures below 11 GPa, and eventually transform to a metastable r8-Ge at 6–8 GPa under hydrostatic conditions [17,25]. Simulations also show that transformation back to energetically more favorable α-Ge is inhibited by higher-enthalpy barriers [10,16]. Despite decades of effort, a couple of questions remain regarding the changes of electronic states across the structural α-β transition: What is the nature of *d* orbitals in β-Ge at pressures below the structural α-β transition pressure at ∼11 GPa? Does the population of *d* orbitals in β-Ge change abruptly or progressively with the gradual increase of covalent bonding upon decompression?

In principle, high-quality single-crystal diffraction data can provide information of EDDs to address these questions. However, when an α-Ge single crystal is compressed at pressures above 11 GPa at room temperature, the single crystal will be destroyed due to the α-β transition with the transformed β-Ge in polycrystalline form [24]. In order to perform single-crystal diffraction studies on β-Ge, we have developed routes to synthesize single crystals or coarse grains of β-Ge in a diamond anvil cell (DAC). We report the experimentally determined EDDs in β-Ge from single-crystal x-ray diffraction (XRD) and multigrain XRD measurements under *in situ* high-pressure conditions. Upon decompression, the participation of *d* orbitals in the valence band in β-Ge is found to decrease abruptly at ∼10–11 GPa, even though the β-Ge samples still remain as single crystals with a high crystallinity. Contrary to the results of α-Ge upon compression [24], where only weak *d* orbitals are observed in the valence level in the stability field of α-Ge at pressures of 7.7–11.0 GPa, the result of β-Ge under decompression

---

*Present address: Center of Correlated Matter, Zhejiang University, Hangzhou, Zhejiang 310058, China.
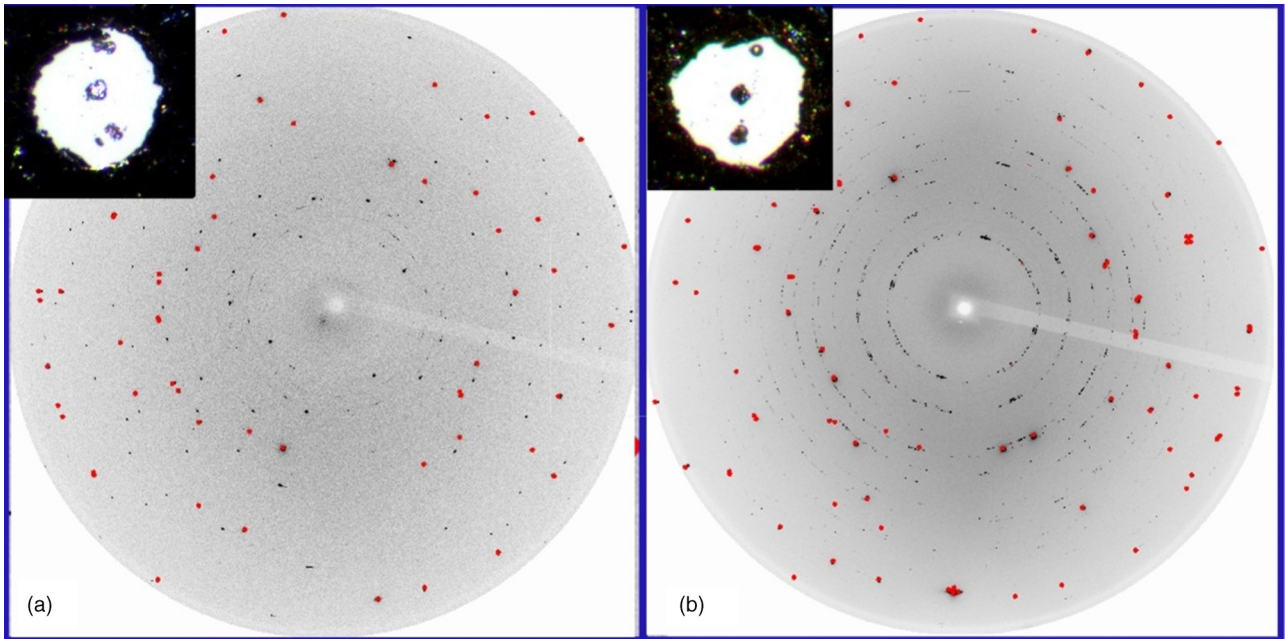†gyshen@anl.gov

FIG. 1. Typical diffraction images of (a) single-crystal β-Ge at 8.7 GPa and (b) multigrain β-Ge at 7.2 GPa. Red dots in the images are the reflections from diamond anvils. The insets are the photos for the corresponding samples, taken under a microscope, showing the Ge samples at the central region with a few ruby balls away from the center. The chamber size in the photos is around 80 μm in diameter.

suggests that a large change in d-orbital participation in bonding can occur in the β-Ge lattice.

II. EXPERIMENTAL PROCEDURES

An α-Ge single-crystal sample (Hefei Kejing Materials Technology) was cut into a rectangular piece of approximately $20 \times 30\,\mu$m^2 and 7 μm thick, and subsequently loaded into a DAC with a large opening angle of $4\vartheta = 60°$. The culet size of the anvils is 300 μm. A 250-μm-thick Re gasket was preindented to 35 μm thick with a hole of 120 μm in diameter at the center of the indentation as the sample chamber. Neon was used as the pressure-transmitting medium. The DAC was loaded together with several small ruby balls for pressure determination by the ruby fluorescence method [26]. The β-Ge samples were obtained by pressurizing α-Ge to above 11 GPa. We subsequently heated the β-Ge samples by applying double-sided laser-heating [27] with a heating spot of ~50 μm in diameter to a temperature ~1000 K for at least 1 min. By gradually decreasing the laser power, the temperature was reduced to room temperature in 50 min. As a result, we obtained a single-crystal β-Ge sample [Fig. 1(a)]. In a separate synthesis, we annealed the polycrystalline β-Ge sample at 13.8 GPa using a resistively heated holder to heat the entire DAC to 633 K for 10 h. After the entire assembly was cooled down to room temperature in about 1 h, the sample pressure changed to 14.2 GPa. The annealed β-Ge sample displayed spotty diffraction patterns suggesting multiple coarse grains of 3–5 μm in size [Fig. 1(b)].

The XRD experiments were performed at the 16-BM-D beamline at the Advanced Photon Source. A monochromatic beam with a wavelength of 0.309 98(3) Å was focused to a beam size of about $5 \times 10\,\mu$m^2 at full width at half maximum (FWHM) in horizontal and vertical directions, respectively.

Three independent single-crystal XRD runs (SC1, SC2, SC3) and two multigrain XRD runs (MG1, MG2) were conducted under compression and decompression pathways, all at room temperature (Fig. 2). The pressure pathways for the SC1, SC2, and SC3 runs were compression from 13.6 to 26.5 GPa, compression from 10.9 to 34.8 GPa followed by decompression from 34.8 GPa to ambient pressure, and decompression from 14.1 to 6.4 GPa, respectively. The pressure pathways for the MG1 and MG2 runs were both under decompression processes from 14.2 and 16.6 GPa to ambient pressure, respectively. A MAR345 imaging plate was used for collecting XRD data, covering a full angle of 50° for XRD. The sample was located above a ω-rotation center, with XRD signals collected at each small increment of the ω rotation. In single-crystal XRD, a step size of 2° was used, while in multigrain XRD, the step size was 1°.

Our data analysis procedure is similar to those used in our previous studies [14,24], with its flow chart shown in Fig. 3. Briefly, the GSE_ADA software [28] was used for the single-crystal XRD data integration and the pixel-by-pixel reciprocal plane reconstructions. In the range of $\frac{\sin\theta}{\lambda} < 0.75$ Å^{-1}, totals of 25, 22, and 28 independent reflections were found in the SC1, SC2, and SC3 runs, respectively. For the multigrain XRD data, we used a custom program developed by ourselves to search the reflections and index the XRD data. A typical procedure of using the program is as follows. We first select a few strong reflections in a given diffraction angle. Then we search all pairs of each reflection from the same grain along the selected diffraction angle. From each observed pair of reflections, we calculate the orientation matrix [29], and subsequently apply the orientation matrix to index all other reflections. Those matrices capable of indexing a reasonable number of reflections are considered to represent the corresponding individual grain. The intensities of reflections from
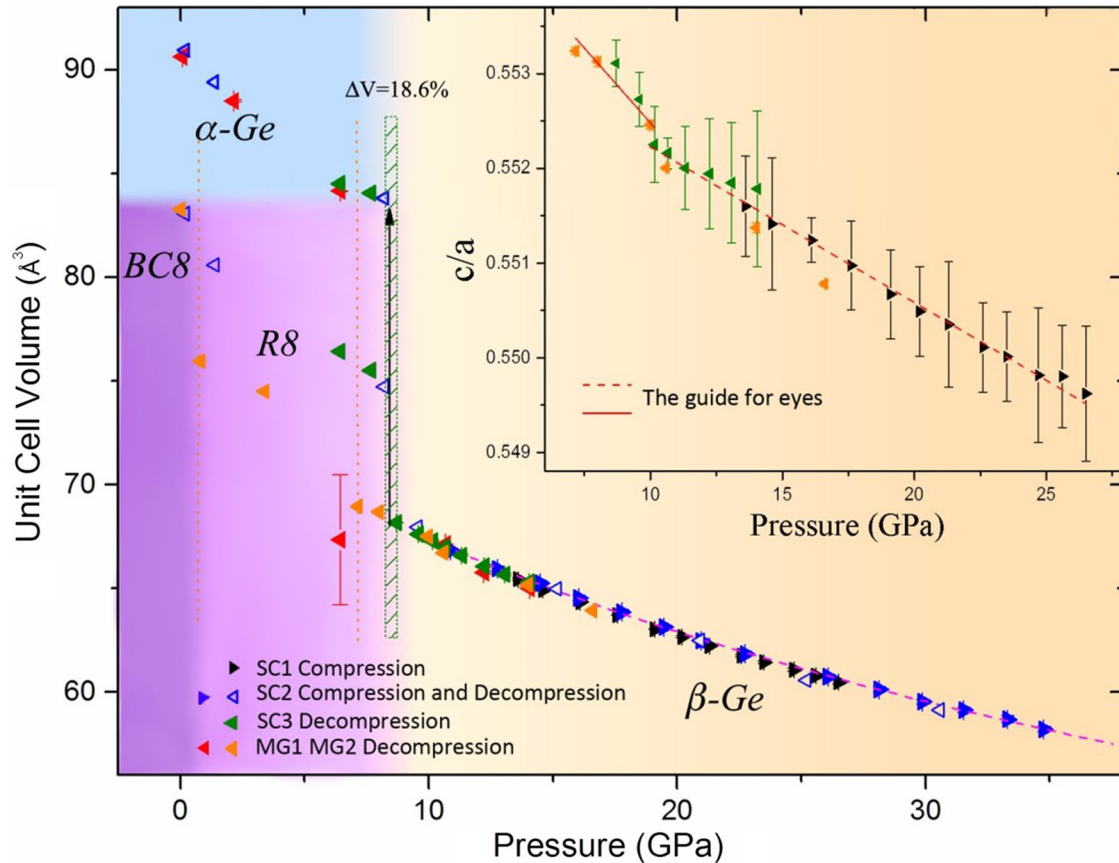
FIG. 2. Pressure dependence of the unit cell volume under compression and decompression for Ge samples. Solid black and blue right-pointing triangles represent two single-crystal compression runs, SC1 and SC2, respectively. Blue open left-pointing triangles and green solid left-pointing triangles represent two single-crystal decompression runs, SC2 and SC3, respectively. Red and orange left-pointing triangles represent the multigrain data from the MG1 and MG2 runs, respectively. The pink dashed line is the fit to the Birch-Murnaghan equation of state, with $K_0 = 61(12)$ GPa, $K' = 5.9(10)$, and $V_0 = 78(11)$ Å^3. The inset shows the pressure dependence of the c/a ratio in β-Ge from the results in the SC1, SC3, and MG2 runs. The lines are a guide for the eyes.

each grain are calculated using the XDS program [30,31]. This process is repeated until most of the reflections are covered. From the collected multigrain data for β-Ge, we found a dozen of individual grains. While the completeness of each grain varies from 50% to 80%, combining all grains provides 100% completeness in the covered reciprocal range, as shown in Table I. The structural refinement for all data was carried out using the SHELX program [32] with R factors lower than 3.2% (Tables II and III). The EDD analysis in β-Ge was performed by the maximum entropy method (MEM) [33] using the software PRIMA [34] with the unit cell divided into $80 \times 80 \times 48$ pixels.

III. RESULTS AND DISCUSSION

As illustrated in Fig. 2, β-Ge is still observed as single crystals at pressures far below 11 GPa upon decompression, and remains so until a structural transformation to metastable Ge phases below ∼8.5 GPa. In contrast to previous observations of a constant c/a ratio (0.547) for β-Ge [12,35,36], our high-precision data from single-crystal XRD show that the c/a ratio increases almost linearly from 0.550 to 0.553 with decreasing pressure, with a subtle, but noticeable, slope change below 10.1 GPa (Fig. 2, inset). In two single-crystal

runs (SC2, SC3), a transition from β-Ge to a mixture of r8-Ge and α-Ge is observed at 8.2–8.5 GPa. Upon further decompression, the r8-Ge transforms to bc8-Ge at ∼1 GPa. The occurrence of metastable phases under decompression of the two multigrain runs are different. In the MG1 run, the multigrain β-Ge is found to transform to pure α-Ge, with XRD intensity uniformly distributed along the diffraction rings, indicating a fine-grained powder for the recovered α-Ge. In the MG2 run, a mixture of st12-Ge and an unknown phase is observed upon pressure release to ambient condition. While the transition pressures from β-Ge to metastable phases are in general agreement with those in the previous studies [2,16,17], the appeared metastable phases under decompression, however, are different from those reported [16,20,21,25,37] which may be partly related to the sample nature of coarse grains and the quasihydrostatic condition in this study.

Figure 4 shows the normalized electron densities in β-Ge, by integrating electron densities between two neighboring Ge atoms along the c axis. To visualize the effect of pressure on the electron density in β-Ge, the differences in EDDs between two pressure points (ΔEDD) are shown in the top line of Fig. 4. It is prudent to point out that the overall uncertainty in EDD from different runs is typically at the 3%–4% level. However, *the change* in EDD with pressure in a single run can
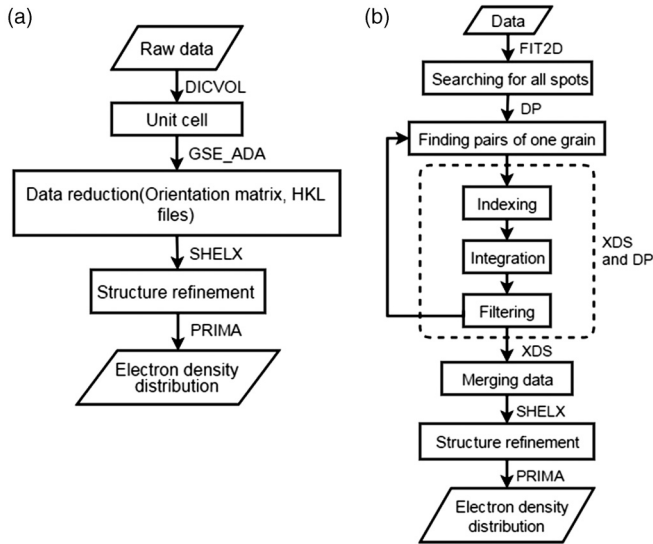
FIG. 3. Flow diagrams of the data analysis procedures in obtaining structural solutions using single-crystal and multigrain diffraction data. (a) For single-crystal diffraction, the intensities of reflections are first obtained by integrating each of the observed diffraction peaks after peak searching and intensity corrections. (b) For multigrain diffraction, we typically start with indexing the reflections from the dominant grains. Then we search for orientation matrices of as many individual grains as possible. After individual grains are identified, the data analysis procedures are similar to those in single-crystal data, such as removing the shadows caused by the DAC and applying filtering, correction, and scaling using the program XDS. Then we merge data from the identified individual grains for structural refinement and the EDDs.
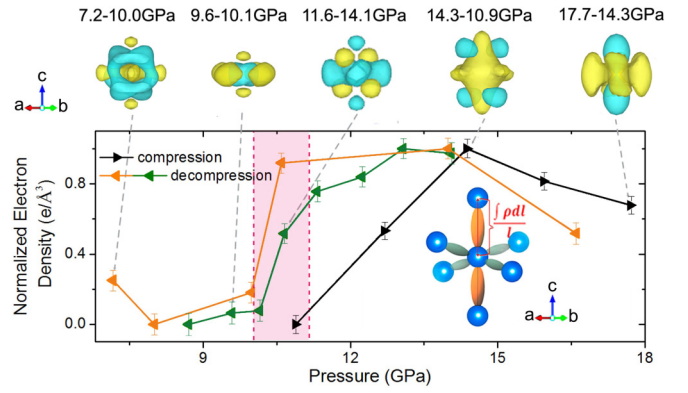

FIG. 4. Normalized electron densities in β-Ge along the c axis. The values are obtained by integrating charge densities between two neighboring atoms along the c axis. The error bars in EDD include statistical errors and a systematic error (fixed at 2.5%) in the algorithm of the maximum entropy method [38]. The black right-pointing triangles represent the compression data from the SC2 run, while the orange and green left-pointing triangles represent decompression data from the MG2 and SC3 runs. Five local deformation electron densities between two different pressures are indicated in the top line. The positive and negative differences are yellow and blue, respectively, with the isosurface level setting at $1\,e/Å^3$.

be determined more precisely than this typical uncertainty of absolute EDD. This is because the experimental conditions at various pressures are almost identical in the pressure range of this study. For the differential EDD, the corrections in data analysis, such as background, polarization, and absorption corrections, are nearly identical for each pressure point. Thus the influences on differential EDDs become negligible, resulting in better precision compared to absolute EDD [24]. Under

compression in the SC2 run (black right-pointing triangles in Fig. 4), electron densities along the c axis increase with increasing pressure and then turn over at $\sim$14.3 GPa. The increase in electron density between 10.9 and 14.3 GPa may be a result of the increased d_{z^2} electrons participating in the bonding upon compression, because the bonding along the c axis is related to the hybridization of s and d_{z^2} electrons near the Fermi level [9]. Above 14.3 GPa, the turnover may be related to the growing delocalization of the electrons (i.e., the increasing metallic character) that may have contributed in the decrease in electron density. Upon decompression in the SC3 run (green left-pointing triangles) and MG2 run (orange left-pointing triangles), the electron density along the c axis increases slightly, first with decreasing pressure to 13.3 GPa (Fig. 4), and then turns to decrease gently with decreasing

TABLE I. Twelve individual grains are used for structure refinement from data at 14.2 GPa in the MG1 run. The completeness reaches 100% in the covered reciprocal space.

Grain	Observed/independent/free reflections	Completeness (%)	R_{int}	R/R_{free}
1	76/26/3	69	0.068	0.055/0.068
2	82/26/4	81	0.097	0.051/0.039
3	79/21/3	74	0.055	0.028/0.024
4	75/30/4	81	0.064	0.040/0.050
5	67/19/3	52	0.075	0.034/0.078
6	59/16/3	55	0.053	0.034/0.053
7	78/32/4	81	0.074	0.048/0.050
8	76/31/4	86	0.055	0.058/0.033
9	63/15/2	43	0.041	0.021/0.017
10	75/21/3	64	0.067	0.031/0.079
11	81/22/1	71	0.051	0.024/0.019
12	82/20/2	74	0.060	0.029/0.020
Combined	870/37/5	100	0.096	0.025/0.031

TABLE II. Experimental conditions and refinement parameters from three single-crystal experiments. Pressure uncertainties are typically ± 0.1 GPa.

SC1 run	P (GPa)	$U11$[a]	$U33$[a]	$R1$[b]	$Rw2$[c]	S[d]	N[e]	R_{int}[f]
	13.6	0.01193	0.01784	0.0206	0.0637	1.171	25	0.0735
	14.6	0.01318	0.01625	0.0248	0.0540	1.336	24	0.0550
	16.1	0.01102	0.01661	0.0215	0.0485	1.595	22	0.0611
	17.6	0.01250	0.01753	0.0191	0.0424	1.122	22	0.0574
	19.1	0.01477	0.01906	0.0236	0.0550	1.277	23	0.0609
	20.2	0.01128	0.01514	0.0280	0.0718	1.406	23	0.0527
	21.3	0.01256	0.01514	0.0191	0.0506	1.169	23	0.0614
	22.5	0.01306	0.01545	0.0196	0.0427	1.232	21	0.0506
	23.5	0.01372	0.01557	0.0273	0.0607	1.339	21	0.0629
	24.6	0.01150	0.01327	0.0284	0.0671	1.022	21	0.0585
	25.6	0.01313	0.01513	0.0299	0.0576	1.060	21	0.0805
	26.5	0.01224	0.01423	0.0243	0.0548	1.171	21	0.0640
SC2 run	P (GPa)	$U11$	$U33$	$R1$	$Rw2$	S	N	R_{int}
	10.9	0.00852	0.01075	0.0126	0.0279	1.418	22	0.0291
	12.9	0.00833	0.01054	0.0092	0.0227	1.235	22	0.0364
	14.3	0.00809	0.01000	0.0212	0.1152	1.238	25	0.0712
	16.2	0.00813	0.00976	0.0146	0.0542	1.256	22	0.0221
	17.7	0.00826	0.01097	0.0156	0.0405	1.251	22	0.0374
SC3 run	P (GPa)	$U11$	$U33$	$R1$	$Rw2$	S	N	R_{int}
	14.1	0.01494	0.01656	0.0190	0.0383	1.159	28	0.0401
	13.1	0.01502	0.01531	0.0190	0.0372	1.382	28	0.0524
	12.2	0.01485	0.01752	0.0212	0.0486	1.343	28	0.0640
	11.3	0.01475	0.01701	0.0242	0.0542	1.256	28	0.0648
	10.7	0.01588	0.01690	0.0241	0.0552	1.166	28	0.0686
	10.2	0.01691	0.01766	0.0291	0.0762	1.291	28	0.0631
	9.6	0.01578	0.01747	0.0324	0.0620	1.214	26	0.0535
	8.5	0.01670	0.01796	0.0294	0.0761	1.216	26	0.0533

[a]U: anisotropic displacement parameters.
[b]$R1$: conventional R values.
[c]$Rw2$: weighted R values.
[d]S: goodness of fit.
[e]N: number of reflections.
[f]R_{int}: merging R values.

pressure down to $\sim$11 GPa. Then, remarkably, there is a sharp decrease in electron density slightly below 11 GPa, a pressure close to the structural α-β transition pressure, while the single-crystal β-Ge samples still display a high crystallinity with sharp XRD spots [as shown in Fig. 1(a)]. This means that significant pressure-induced electronic changes can occur within the β-Ge lattice. The abrupt change in electron density suggests that there must exist a sudden weakening of metallic bonds in β-Ge at 10–11 GPa. The observed subtle change in the c/a ratio below 10.1 GPa (the inset of Fig. 2) may be a signature in crystal structure caused by the sudden change in electron density, because the reduced participation of d electrons may have caused the slightly enlarged distance along the c axis.

Thus, even though β-Ge can exist below 10 GPa under decompression, it must be viewed as metastable because at heart its electron topology has already dramatically changed. This indicates that the electronic changes (d_{z^2} orbital contribution) provide a pretransition process in the phase transition

from β-Ge to metastable Ge phases under decompression. The intrinsic anisotropy in the orientational configuration of the d_{z^2} orbital in tetragonal β-Ge may kinetically influence the transformation to orientation-matched metastable phases. The path-dependent metastability upon decompression [16,17] of β-Ge supports that they are kinetically controlled, rather than thermodynamically driven.

Indeed, the obtained EDD maps reveal electronic contributions of structural phase transitions from β-Ge to metastable Ge phases. For example, in the SC3 and MG1 runs under decompression, β-Ge transforms to a different metastable phase with a mixture of α-Ge and r8-Ge in the SC3 run and pure α-Ge in the MG1 run. Because the two nearest atoms in r8-Ge correspond to nearest neighboring atoms in the (110) plane in β-Ge [16], we plot EDD maps in the (110) plane (Fig. 5). An increased EDD is observed between two nearest neighboring atoms under decompression below 10.7 GPa in the SC3 run [Fig. 5(a)], while no obvious EDD changes are observed for the MG1 run [Fig. 5(b)]. The increased EDD

TABLE III. Experimental conditions and refinement parameters from two multigrain experiments. Pressure uncertainties are typically ± 0.1 GPa.

MG1	P (GPa)	N_{tot}	N_{ref}	$R1$	R_{free}	R_{int}	S	$U11$	$U33$
	14.2	870	37	0.0253	0.0312	0.0961	0.847	0.01108	0.01401
	12.2(1)	826	36	0.0226	0.0147	0.0859	0.422	0.01131	0.01268
	10.6	902	38	0.0266	0.0528	0.0827	0.658	0.01204	0.01329
	7.6	763	37	0.0233	0.0322	0.0869	0.572	0.01064	0.01294
MG2	P (GPa)	N_{tot}[a]	N_{ref}[b]	$R1$[c]	R_{free}[d]	R_{int}[e]	S[f]	$U11$[g]	$U33$[g]
	16.6	490	31	0.0202	0.0203	0.0649	1.166	0.01387	0.01600
	14.0	667	37	0.0226	0.0339	0.0613	1.322	0.01044	0.01254
	10.6	710	39	0.0289	0.0365	0.0479	1.208	0.01226	0.01530
	10.0	548	33	0.0319	0.0230	0.0785	1.315	0.01366	0.01623
	8.0	496	36	0.0316	0.0678	0.0807	1.406	0.01353	0.01677
	7.2	487	37	0.0279	0.0322	0.0612	1.226	0.01265	0.01478

[a]N_{tot}: total number of the reflections.
[b]N_{ref}: number of independent reflections.
[c]$R1$: conventional R values.
[d]R_{free}: crystallographic free R values.
[e]R_{int}: merging R values.
[f]S: goodness of fit.
[g]U: anisotropic displacement parameters.

along the nearest neighbors in the (110) plane in β-Ge may be associated with the appearance of r8-Ge below 8.5 GPa in the SC3 run. On the other hand, the lack of EDD change may
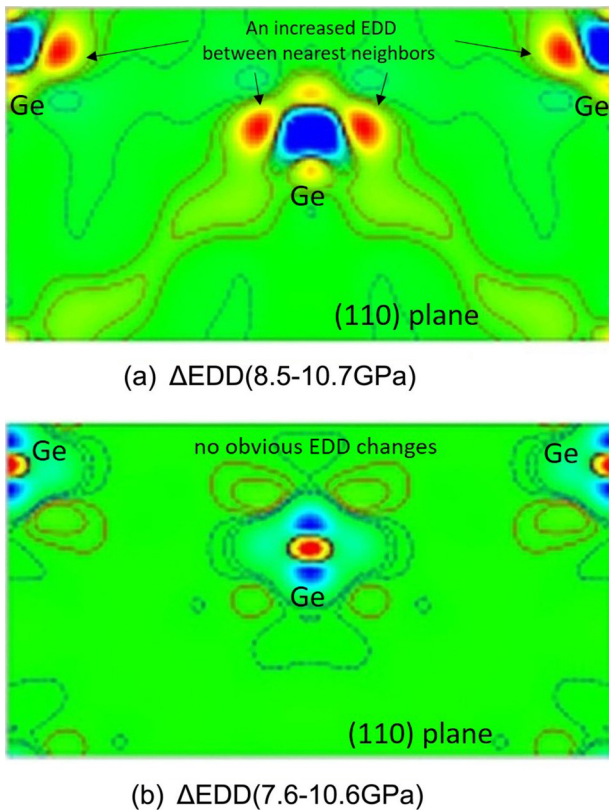

(a) ΔEDD(8.5-10.7GPa)

(b) ΔEDD(7.6-10.6GPa)

FIG. 5. Two-dimensional differential electron density distribution maps of β-Ge in two runs, SC3 (a) and MG1 (b) along the (110) plane. Positive and negative differences are drawn as red solid and blue dotted lines, respectively.

be related to the formation of the pure α-Ge below 7.6 GPa in the MG1 run.

The changes of d-electron participation in bonding should have a signature in the metallic character of the Ge samples. To test this, we have conducted infrared reflectance measurements at room temperature using a Bruker Vertex 80 V FT-IR spectrometer (Bruker Optik GmbH, Germany) equipped with a nitrogen-cooled HgCdTe detector. In order to avoid interference noise, a slice of the Ge sample was directly attached to a culet surface of the diamond anvil without a pressure medium. Pressure-dependent reflectance spectra were measured at the interface between the sample and the diamond anvil. The spectrum of an empty cell served as the reference to normalize the reflectance spectra. As can be seen in Fig. 6, the reflectance of α-Ge is nearly constant up to 7 GPa, above which the reflectance increases gradually with increasing pressure, corresponding to the increased participation of d electrons in the valence band near the Fermi level [24]. At $\sim$11 GPa, the reflectance sharply increases corresponding to the semiconducting-metallic transition to β-Ge. At pressures above 15 GPa, the reflectance maintains at a certain level. Upon decompression, the reflectance of β-Ge sharply decreases at $\sim$10.5 GPa. The decreasing rate slows down between 9.5 and 7 GPa, and then the reflectance becomes nearly constant with decreasing pressure. Overall, the general trend of the reflectance changes is correlated with the participation of d electrons in bonding.

By combining the current results of β-Ge with the previous work on α-Ge [24], we can illustrate a summary on the pariciaption of d electrons in bonding under compression and decompression across the α-β transition. Upon compression of α-Ge, the sp^3 bonding is enhanced with increasing pressure up to 7.7 GPa, above which, but below the α-β transition pressure of $\sim$11 GPa, an increased participation of d electrons in the valence band occurs in α-Ge. However, the participation of d electrons in the stability field of α-Ge remains
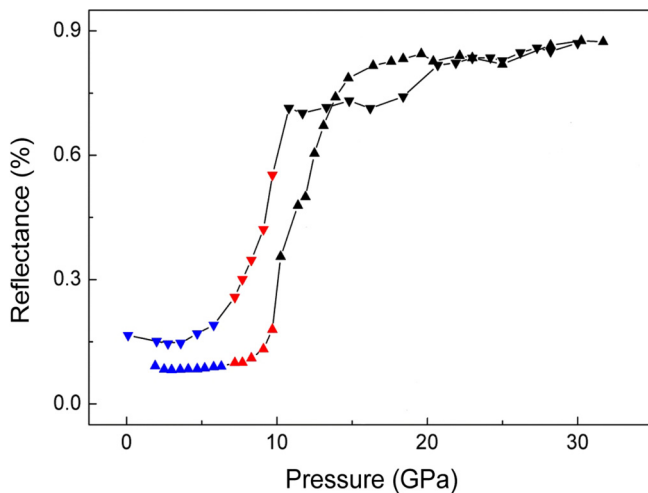
FIG. 6. Reflectance of Ge as a function of pressure measured by infrared spectroscopy under compression and decompression shown as upward triangles and downward triangles, respectively. The inset shows an enlarged plot at pressures below 11 GPa.

relatively small. On the other hand, upon decompression of β-Ge, there are rich changes in d-orbital participation in bonding. First, a gradual decrease of d-electron participation in β-Ge occurs from ~14 to ~11 GPa. At pressure slightly below ~11 GPa, there appears an abrupt decrease in d-orbital participation. At pressures below ~10 GPa, there is another gradual decrease of d electrons until there is a transformation from β-Ge to metastable Ge phases. It is interesting to note that the abrupt electronic changes happen at pressures around 10–11 GPa, only slightly below the structural α-β transition pressure near 11 GPa. Thus under decompression pathways, β-Ge may have largely lost its metallic character at pressure below 10 GPa, even though its single-crystal nature remains intact with a good crystallinity displaying sharp diffraction spots. The fact that β-Ge lattice can host

significant electronic changes may be related to its mixed bonded network with four covalent bonds along the ab plane and two metallic bonds along the c direction. This is in contrast to the covalently bonded case for α-Ge which displays only a weak participation of d electrons under compression above 7.7 GPa. These results imply that β-tin structured materials *at pressures below their stability field* may show intriguing electronic and optical properties. This provides a route for novel materials with large fluctuations in electronic properties in Group IV elements (Si, Ge, α-Sn), III-V compounds (GaP, AlSb, GaSb, InSb, GaAs), and II-VI compounds (ZnS, ZnSe, CdTe) with pressure (or chemical pressure) as an effective controlling parameter. Other stimuli, such as photons and electric and magnetic fields, may also influence the electronic fluctuation in the metastable β-tin structured materials.

[1] J. R. Chelikowsky, Phys. Rev. B **35**, 1174 (1987).

[2] A. Mujica, Rev. Mod. Phys. **75**, 863 (2003).

[3] R. J. Nelmes, M. I. McMahon, P. D. Hatton, J. Crain, and R. O. Piltz, Phys. Rev. B **48**, 9949 (1993).

[4] M. Mezouar, H. Libotte, S. Députier, T. Le Bihan, and D. Häusermann, Phys. Status Solidi B **211**, 395 (1999).

[5] A. Morita and T. Soma, Solid State Commun. **11**, 927 (1972).

[6] J. C. Jamieson, Science **139**, 762 (1963).

[7] J. Phillips, Phys. Rev. Lett. **27**, 1197 (1971).

[8] J. Tse and E. Boldyreva, in *Modern Charge-Density Analysis*, edited by C. Gatti and P. Macchi (Springer Netherlands, Dordrecht, 2012), p. 573.

[9] R. Biswas and M. Kertesz, Phys. Rev. B **29**, 1791 (1984).

[10] M. T. Yin and M. L. Cohen, Phys. Rev. B **26**, 5668 (1982).

[11] Y. K. Vohra, K. E. Brister, S. Desgreniers, A. L. Ruoff, K. J. Chang, and M. L. Cohen, Phys. Rev. Lett. **56**, 1944 (1986).

[12] N. E. Christensen and M. Methfessel, Phys. Rev. B **48**, 5797 (1993).

[13] S. P. Lewis and M. L. Cohen, Phys. Rev. B **48**, 3646 (1993).

[14] D. Selli, I. A. Baburin, R. Martonak, and S. Leoni, Sci Rep **3**, 1466 (2013).

[15] H. Katzke, U. Bismayer, and P. Toledano, Phys. Rev. B **73**, 134105 (2006).

[16] J.-T. Wang, C. Chen, H. Mizuseki, and Y. Kawazoe, Phys. Rev. Lett. **110**, 165503 (2013).

[17] B. Haberl, M. Guthrie, B. D. Malone, J. S. Smith, S. V. Sinogeikin, M. L. Cohen, J. S. Williams, G. Shen, and J. E. Bradby, Phys. Rev. B **89**, 144111 (2014).

[18] A. Di Cicco, A. C. Frasini, M. Minicucci, E. Principi, J.-P. Itiè, and P. Munsch, Phys. Status Solidi B **240**, 19 (2003).

[19] R. J. Nelmes, M. I. McMahon, N. G. Wright, D. R. Allan, and J. S. Loveday, Phys. Rev. B **48**, 9883 (1993).

[20] S. B. Qadri, E. F. Skelton, and A. W. Webb, J. Appl. Phys. **54**, 3609 (1983).

[21] C. S. Menoni, J. Z. Hu, and I. L. Spain, Phys. Rev. B **34**, 362 (1986).

[22] B. D. Malone and M. L. Cohen, Phys. Rev. B **86**, 054101 (2012).

[23] J. S. Kasper and R. H. Wentorf, Jr., Science **197**, 599 (1977).

[24] R. Li, J. Liu, L. Bai, J. S. Tse, and G. Shen, Appl. Phys. Lett. **107**, 072109 (2015).

[25] B. C. Johnson, B. Haberl, S. Deshmukh, B. D. Malone, M. L. Cohen, J. C. McCallum, J. S. Williams, and J. E. Bradby, Phys. Rev. Lett. **110**, 085502 (2013).

[26] H. K. Mao, J. Xu, and P. M. Bell, J. Geophys. Res. **91**, 4673 (1986).

[27] Y. Meng, R. Hrubiak, E. Rod, R. Boehler, and G. Shen, Rev. Sci. Instrum. **86**, 072201 (2015).

[28] P. Dera, GSE_ADA data analysis program for monochromatic single crystal diffraction with area detector, 2007.

[29] W. R. Busing and H. A. Levy, Acta Crystallogr. **22**, 457 (1967).

[30] W. Kabsch, Acta Crystallogr., Sect. D **66**, 125 (2010).

[31] W. Kabsch, Acta Crystallogr., Sect. D **66**, 133 (2010).

[32] G. Sheldrick, Acta Crystallogr., Sect. A **64**, 112 (2008).

[33] W. Jauch and A. Palmer, Acta Crystallogr., Sect. A **49**, 590 (1993).

[34] F. Izumi and T. Ikeda, in *European Powder Diffraction, Parts 1 and 2*, edited by R. Delhez and E. J. Mittemeijer (Trans Tech Publications Ltd, Zurich-Uetikon, Switzerland, 2000), p. 198.

[35] A. Mujica, S. Radescu, and R. J. Needs, J. Phys.: Condens. Matter **13**, 35 (2001).

[36] X.-J. Chen, C. Zhang, Y. Meng, R.-Q. Zhang, H.-Q. Lin, V. V. Struzhkin, and H.-k. Mao, Phys. Rev. Lett. **106**, 135502 (2011).

[37] F. Coppari, J. C. Chervin, A. Congeduti, M. Lazzeri, A. Polian, E. Principi, and A. Di Cicco, Phys. Rev. B **80**, 115213 (2009).

[38] L. Dobrzyński and J. Waliszewski, J. Phys. Soc. Jpn. **72**, 2203 (2003).